

# *BeppoSAX* Spectral Survey of BL Lacs - new spectra and results

V. Beckmann<sup>1,2</sup>, A. Wolter<sup>3</sup>, A. Celotti<sup>4</sup>, L. Costamante<sup>3</sup>, G. Ghisellini<sup>3</sup>, T. Maccacaro<sup>3</sup>, and G. Tagliaferri<sup>3</sup>

<sup>1</sup> INTEGRAL Science Data Centre, Chemin d' Ecogia 16, CH-1290 Versoix, Switzerland

<sup>2</sup> Institut für Astronomie und Astrophysik, Universität Tübingen, Sand 1, D-72076 Tübingen, Germany

<sup>3</sup> Osservatorio Astronomico di Brera, Via Brera 28, I-20121 Milano, Italy

<sup>4</sup> SISSA/ISAS, Via Beirut 2-4, I-34014 Trieste, Italy

Received date; accepted date

**Abstract.** We present *BeppoSAX* LECS, MECS, and PDS spectra of eleven X-ray selected BL Lacertae objects. Combining these sources with the ones presented elsewhere we have a sample of 21 BL Lacs from the Einstein Medium Sensitivity and Einstein Slew Survey. The sample shows strong correlations of several physical parameters with the peak frequency of the synchrotron branch of the spectral energy distribution. In particular the peak frequency is correlated to the X-ray spectral shape: objects with the peak near to the X-ray band show harder and straighter X-ray spectra than those of the low energy peaked sources. This work shows that the recently proposed unification scenario for different types of blazars can hold also within the class of high frequency peaked BL Lac objects.

**Key words.** BL Lacertae objects: general - X-rays: galaxies

## 1. Introduction

BL Lac objects mark one extreme population of active galactic nuclei (AGN). They exhibit intense variability (e.g. Wagner & Witzel 1995) and polarization (e.g. Kühn & Schmidt 1990) but do not show strong emission or absorption lines in their spectrum (e.g. Stocke et al. 1991). In order to understand their physical nature through the emission processes involved and their relative contribution, one has to study their spectral energy distribution (SED).

Determining the SED is a telescope time consuming issue. There exist some well studied bright BL Lac objects - like Mkn 421, 1ES 2344+512 and Mkn 501 - for which detailed measurements at several wavelengths are available, but to construct a global scenario for BL Lac objects it is necessary to also derive the properties of complete samples. This means investigating fainter objects too. Because of its sensitivity and wide energy band, which allows us to study simultaneously the BL Lac spectrum from 0.1 to 100 keV, the *BeppoSAX* satellite is a powerful tool for this aim.

Here we present a well defined sample of 21 BL Lac objects which have been studied using *BeppoSAX*. In the following Section 2 we define the sample; observations and data analysis are explained in Section 3. The X-ray data are compared to earlier results by the ROSAT satellite in

Section 4, and in Section 5 we examine the properties of the BL Lac SEDs. The results are discussed in the context of unified schemes for BL Lac objects in Section 6.

## 2. The sample

Because strong emission lines are missing in the optical spectra of BL Lac objects, this kind of AGN is usually selected either in the radio or in the X-ray band. The X-ray selected BL Lacs are mainly found in the surveys carried out by the *EINSTEIN IPC* (the EMSS Sample, Gioia et al. 1990, and the Slew Survey Sample, Perlman et al. 1996), and by the *ROSAT PSPC* (ROSAT All-Sky Survey Sample; Bade et al. 1998, Beckmann 2000). The Slew Survey Sample covers the whole high Galactic latitude sky, while the EMSS is deeper, but only over an area of  $\sim 800 \text{ deg}^2$ . By selecting objects with fluxes  $F_X(0.1 - 10 \text{ keV}) \geq 10^{-11} \text{ erg cm}^{-2} \text{ sec}^{-1}$  in the Slew Survey and  $F_X \geq 4 \times 10^{-12} \text{ erg cm}^{-2} \text{ sec}^{-1}$  in the EMSS we obtain a sample that combines the advantage of a flux limited sample with a wide coverage of the (spectral) parameter space and thus offers a representative subset of the BL Lac population. This allows us to include several "flavors" of BL Lac objects, ranging from the extreme X-ray dominated HBL to the borderline objects of intermediate BL Lac objects (IBL). The objects we analyse here are the second half of the sample, while the first 10 ob-

**Table 1.** The objects of the sample

Name	R.A. (2000.0)	Dec.	Redshift
1ES 0145+138	01 48 29.8	+14 02 16	0.125
1ES 0323+022	03 26 13.9	+02 25 15	0.147
1ES 0507−040	05 09 38.2	−04 00 46	0.304
1ES 0927+500	09 30 37.6	+49 50 26	0.186
1ES 1028+511	10 31 18.5	+50 53 34	0.361
1ES 1118+424	11 20 48.0	+42 12 10	0.124
1ES 1255+244	12 57 31.9	+24 12 39	0.141
1ES 1533+535	15 35 00.7	+53 20 38	0.890
1ES 1544+820	15 40 15.6	+81 55 04	?
1ES 1553+113	15 55 43.2	+11 11 20	0.360
1ES 1959+650	20 00 00.0	+65 08 56	0.047

jects have been presented in Wolter et al. (1998), hereafter W98.

### 3. *BeppoSAX* Observations and Data Analysis

The X-ray observations have been carried out with *BeppoSAX*, a project of the Italian Space Agency (ASI) with a participation of the Netherlands Agency for Aerospace (NIVR). A detailed description of the entire *BeppoSAX* mission can be found in Butler & Scarsi (1990) and Boella et al. (1997a). The data presented here are from the Low Energy Concentrator Spectrometer (LECS), the Medium Energy Concentrator Spectrometer (MECS), and the Phoswich Detector System (PDS).

The LECS is sensitive in the 0.1–10 keV range with a field of view of 37 arcmin diameter (Parmar et al. 1997). The LECS data are useful up to 4 keV only, because the response matrix is not well calibrated above this energy (Orr et al. 1998). It has an energy resolution of a factor  $\sim 2.4$  better than the *ROSAT PSPC* (Brinkmann 1991), while the effective area is between  $\sim 6$  and 2 times lower at 0.28 and 1.5 keV, respectively.

The MECS has a field of view of 56 arcmin diameter, works in the energy range 1.3–10 keV with an energy resolution of  $\sim 8\%$  and an angular resolution of  $\sim 0.7$  arcmin (FWHM) at 6 keV. The effective area at 6 keV is  $155 \text{ cm}^2$  (Boella et al., 1997b).

The PDS is sensitive in the 13–200 keV band. All photons within the field of view are counted, with no spatial information (f.o.v. diameter  $\sim 1.3$  deg FWHM). Thus other sources in the vicinity of the target can contaminate the measurement.

The 11 objects presented here (for positions and redshifts see Tab. 1) have been observed between May 1997 and February 1999. The data have been pre-processed at the *BeppoSAX* SDC (Science Data Center) and retrieved through the SDC archive. Table 2 shows the journal of observations, including exposure times and net count rates for the LECS, MECS, and PDS detectors.

#### 3.1. Spectral Analysis

For observations accomplished in May 1997 all three MECS units are available, while after this date only MECS units 2 and 3 were in use. The spectra from the MECS units have been summed together to increase the S/N. None of the sources shows extension neither in the LECS nor in the MECS image. The same reduction process as in W98 has been applied to the data, using FTOOLS v4.0 and XSPEC v.9.0 (Shafer et al. 1991).

We fitted simultaneously LECS and MECS data, leaving free the LECS normalization with respect to the MECS to account for the residual errors in the intensity cross-calibration. A reliable value for the ratio should be  $LECS/MECS \sim 0.7 \pm 0.2$  (see the cookbook for *BeppoSAX* scientific analysis under <http://www.asdc.asi.it/bepposax/software/cookbook/> and check the NFI flux cross-calibration). For all sources where PDS data were available they were also simultaneously fitted: only for 1ES 1255+244 there are no PDS data and for 1ES 0145+138 the exposure time was too short to allow a detection in the PDS. The PDS/MECS inter-calibration was handled as a free parameter. In all cases the consideration of the PDS part of the spectrum did not change significantly the results of the spectral analysis, also when fixing the inter-calibration to the value of  $PDS/MECS \sim 0.8$  as recommended by the *BeppoSAX* cookbook. In most cases the statistics of the PDS was not high, as can be seen from the net counts and errors given in Table 2.

The assumed spectral model is a single-power law plus free low energy absorption (arising from cold material with solar abundances; Morrison & McCammon 1983). For all objects we then checked whether a broken-power law with  $N_H$  fixed to the Galactic value would give a significantly better result (as measured by an F-test value greater than 95%) than the single-power law fit, and in five cases indeed the fit improves.

We list the best fit parameters for the cases where the single power law or broken-power law model gave the better fit in Table 3 and Table 4, respectively. Galactic hydrogen column values were taken from the Leiden/Dwingeloo Survey (Hartmann & Burton 1997) and are listed for reference. The errors are 90% confidence levels, for three interesting parameters ( $N_H$ ,  $\alpha_X$ , and normalization). Fluxes in the 2–10 keV band and also in the 0.5–2.0 keV band (for comparison with ROSAT-PSPC fluxes) are given. Also listed are the normalization factors of the LECS relative to the MECS. For the broken-power law we used the  $LECS/MECS$  ratio as determined from the single-power law fit and fixed  $N_H$  to the Galactic value.

We then also checked if a broken-power law model with free fitted absorption would give a better representation of the spectra. This model increases the number of fit parameters and therefore the complexity of the fit. Nonetheless we find all free fitted  $N_H$  values lying in between the Galactic value and that from the single-power

**Table 2.** Journal of *BeppoSAX* observations

Name	obs. date	LECS	LECS	MECS	MECS	PDS	PDS
		exp. time [sec]	net counts	exp. time [sec]	net counts	exp. time [sec]	net counts
1ES 0145+138	30-31/12/97	10576	73.0 ± 9.5	12443	78.7 ± 11.0	-	-
1ES 0323+022	20/01/98	6093	201.6 ± 14.5	14408	607.4 ± 27.2	6845	256 ± 561
1ES 0507-040	11-12/02/99	9116	441.6 ± 21.5	20689	1460.2 ± 40.4	9094	1515 ± 633
1ES 0927+500	25/11/98	8436	568.4 ± 24.3	22712	1967.3 ± 46.5	10129	692 ± 571
1ES 1028+511	1-2/05/97	4552	737.9 ± 28.1	12622	2448.7 ± 50.2	9484	2763 ± 718
1ES 1118+424	1/5/97	6027	236.5 ± 15.6	9982	541.3 ± 24.1	8496	170 ± 147
1ES 1255+244	20/6/98	2484	297.1 ± 17.4	6910	1037.9 ± 33.1	-	-
1ES 1533+535	13-14/02/99	8321	319.4 ± 18.5	26773	931.6 ± 35.5	4056	308 ± 285
1ES 1544+820	13/02/99	8043	170.7 ± 13.6	23249	510.8 ± 26.9	10414	780 ± 363
1ES 1553+113	5/02/98	4421	1179.5 ± 34.5	10618	2157.6 ± 47.3	4671	542 ± 363
1ES 1959+650	4-5/05/97	2252	423.2 ± 20.7	12389	3243.4 ± 57.6	7348	830 ± 516

**Table 3.** *BeppoSAX* : Best fit results for a single-power law model with free fitted  $N_H$ 

Name	Energy	$N_H^a$	$N_H^a$	$F_X^b$	$F_X^c$	Nm <sup>d</sup>	$\chi^2_\nu(dof)$	Prob.
	Index $\alpha_X$	(Gal)	(Fit)	2-10	0.5-2			
0145+138	1.50 <sup>+0.94</sup> <sub>-0.68</sub>	4.59	10.4 <sup>+27.6</sup> <sub>-8.9</sub>	0.35	0.45	0.86	0.38 (3)	77%
0323+022	1.58 <sup>+0.23</sup> <sub>-0.21</sub>	7.27	31.6 <sup>+14.6</sup> <sub>-11.5</sub>	2.24	1.93	0.81	0.51 (27)	98%
0507-040	1.14 <sup>+0.12</sup> <sub>-0.11</sub>	7.84	14.5 <sup>+7.8</sup> <sub>-5.6</sub>	3.88	2.72	0.82	0.73 (69)	95%
1028+511	1.32 <sup>+0.08</sup> <sub>-0.07</sub>	1.27	3.7 <sup>+0.8</sup> <sub>-0.7</sub>	10.10	12.50	0.66	0.85 (97)	85%
1544+820	2.13 <sup>+0.29</sup> <sub>-0.26</sub>	3.70	20.1 <sup>+11.3</sup> <sub>-8.2</sub>	0.95	2.06	0.63	0.68 (30)	90%
1959+650	1.64 <sup>+0.08</sup> <sub>-0.08</sub>	0.99	25.5 <sup>+7.1</sup> <sub>-6.0</sub>	12.90	13.52	0.65	0.79 (88)	92%

<sup>a</sup> hydrogen column density in  $\times 10^{20} \text{cm}^{-2}$

<sup>b</sup> un-absorbed flux in  $10^{-12} \text{erg cm}^{-2} \text{sec}^{-1}$  in the 2–10 keV MECS energy band

<sup>c</sup> un-absorbed flux in  $10^{-12} \text{erg cm}^{-2} \text{sec}^{-1}$  in the 0.5–2.0 keV LECS energy band

<sup>d</sup> Normalization of LECS versus MECS

**Table 4.** *BeppoSAX* : Best fit results for a broken-power law model applying Galactic  $N_H$  values, when significantly better representation of the data than the single power-law (according to an F-test). For comparison, also the results for single-power law with free fitted  $N_H$  are given. The description of the various columns is as in Table 3

Name	Energy	$\alpha_1$	$\alpha_2$	$E_0$	$N_H^a$	$N_H^a$	$F_X^b$	$F_X^c$	Nm <sup>d</sup>	$\chi^2_\nu(dof)$	Prob.
	Index $\alpha_X$			[keV]	(Gal)	(Fit)	2-10	0.5-2			
0927+500	1.18 <sup>+0.09</sup> <sub>-0.09</sub>	0.40 <sup>+0.18</sup> <sub>-0.23</sub>	1.27 <sup>+0.08</sup> <sub>-0.08</sub>	1.35 <sup>+0.28</sup> <sub>-0.24</sub>	1.31	4.3 <sup>+1.3</sup> <sub>-0.9</sub>	4.59	4.59	0.69	0.88 (61)	74%
1118+424	1.57 <sup>+0.16</sup> <sub>-0.16</sub>	1.43 <sup>+0.08</sup> <sub>-0.10</sub>	3.43 <sup>+0.7</sup> <sub>-0.7</sub>	5.11 <sup>+1.6</sup> <sub>-2.3</sub>	2.59	3.5 <sup>+1.3</sup> <sub>-1.0</sub>	2.55	3.65	0.57	0.78 (23)	76%
1255+244	1.15 <sup>+0.12</sup> <sub>-0.11</sub>	0.61 <sup>+0.19</sup> <sub>-0.37</sub>	1.23 <sup>+0.13</sup> <sub>-0.04</sub>	1.58 <sup>+0.36</sup> <sub>-0.36</sub>	1.21	3.6 <sup>+1.5</sup> <sub>-1.0</sub>	8.03	7.81	0.74	0.78 (36)	83%
1533+535	1.57 <sup>+0.15</sup> <sub>-0.14</sub>	0.68 <sup>+0.19</sup> <sub>-0.25</sub>	1.74 <sup>+0.16</sup> <sub>-0.15</sub>	1.40 <sup>+0.30</sup> <sub>-0.27</sub>	1.28	4.8 <sup>+1.9</sup> <sub>-1.1</sub>	1.64	2.89	0.71	0.96 (44)	55%
1553+113	1.79 <sup>+0.09</sup> <sub>-0.08</sub>	0.57 <sup>+0.18</sup> <sub>-0.22</sub>	1.85 <sup>+0.09</sup> <sub>-0.08</sub>	1.13 <sup>+0.90</sup> <sub>-0.90</sub>	3.53	9.2 <sup>+2.3</sup> <sub>-1.3</sub>	9.37	19.16	0.76	1.05 (89)	35%

law and only in one case (1ES 1959+650) the free  $N_H$  from the broken-power law is in better agreement with the fitted  $N_H$  from the single-power law than with the Galactic value. Because of that we assumed that in the broken-power law model there is no significant low energy absorption in the source other than that approximated by the Galactic neutral hydrogen column. We thus have five free parameters in both models. For the single power law with free fitted absorption the spectral slope  $\alpha_X$ , the absorption  $N_H$ , the LECS/MECS and the PDS/MECS normalization, and normalization of MECS. Although for the broken-power-law we added two more free parameters, i.e. the break energy  $E_0$  and the second spectral index  $\alpha_2$ , we fixed column density  $N_H$  to the Galactic value and the *LECS/MECS* normalization to the same value found previously for the single power law. All broken-power laws

show a flat slope in the low energy range ( $\alpha_1 = 0.4 - 0.7$ ) and a steep high energy tail ( $\alpha_2 = 1.2 - 1.9$ ) with a break energy within the LECS energy band ( $E_0 = 1.1 - 1.6$  keV), except 1ES 1118+424 ( $E_0 = 5.1$  keV).

As mentioned, all sources except 1ES 1255+244 and 1ES 0145+138 have been also detected (at  $\geq 4\sigma$ ) in the PDS. In all cases the single- or broken- power law fit give a good approximation of the spectrum in the energy range  $0.1 \leq E \leq 30$  keV and even up to 100 keV in the case of 1ES 1028+511.

The *BeppoSAX* data and best fits are plotted in Figure 1.

Before concluding this section, we would like to point out the presence of a possible feature in the SAX spectrum of 1ES 0927+500. For all models it shows a significant excess within the LECS 1.3 – 1.5 keV energy range.

For an added Gaussian line, the fit gives a central energy  $E = 1.4 \pm 0.1$  keV, corresponding to a rest frame energy of  $\sim 1.7$  keV, and a line width of  $FWHM \simeq 200$  eV, comparable to the energy resolution of the LECS at this energy (F-test probability 99.9%). Since the significance of the detection is low and the energy does not have an obvious physical identification, we refrain from further analysis until new data will be available.

#### 4. Comparison with ROSAT PSPC data

Four of the 11 sources studied here have also been observed during *ROSAT* PSPC pointed observations and for ten of the sources<sup>1</sup> data are available from the ROSAT All Sky Survey Bright Source Catalogue (RASS-BSC; Voges et al. 1999).

In order to compare the ROSAT and *BeppoSAX* results we estimated the best fitting values for spectral slope and absorption from the ROSAT spectra. For the RASS-BSC data we used the hardness ratios, a method described by Schartel et al. (1996), where the hardness ratio is defined as  $HR = \frac{H-S}{H+S}$  with  $H$  and  $S$  being the number of counts in the hard and soft energy bands; typically two ratios are computed: *HR1* with energy ranges  $S = 0.1 - 0.4$  keV and  $H = 0.5 - 2.0$  keV, and *HR2* with  $S = 0.5 - 0.9$  keV and  $H = 1.0 - 2.0$  keV (Voges et al. 1999). The values for the hardness ratios range by definition from -1 for extremely hard to +1 for very soft X-ray spectra. The error estimate for the  $N_H$  and  $\alpha_X$  values is based on the hardness ratios only, not on the photon spectrum itself. Therefore this method does not give  $\chi^2$  values, but is able to determine 68%( $1\sigma$ ) errors. This is done by exploring the hardness-ratio, spectral slope, and  $N_H$  parameter space, determining the  $1\sigma$  region within it for a given set of parameter components. For the pointed observations we instead used the standard reduction procedure as described e.g. in Comastri, Molendi & Ghisellini (1995).

For all objects we considered two models, namely a single-power law with either free fitted absorption or absorption fixed at the Galactic value. For the pointed observations the model with free absorption gives acceptable results; however the exposure time for the RASS-BSC data is quite short and thus we used the values derived from the single-power law model with Galactic absorption. The results are reported in Tables 5 and 6, respectively.

##### 4.1. Comparison between *BeppoSAX* and ROSAT results

We made a comparison of the fluxes between the *ROSAT* PSPC and the *BeppoSAX* observations. To do so, we used the fluxes in the 0.5–2 keV energy band, that is inside both the ROSAT/PSPC and LECS energy ranges. They vary

<sup>1</sup> The flux of 1ES 0145+138 is too low to be included in the RASS-BSC and thus we do not have ROSAT data for this object.

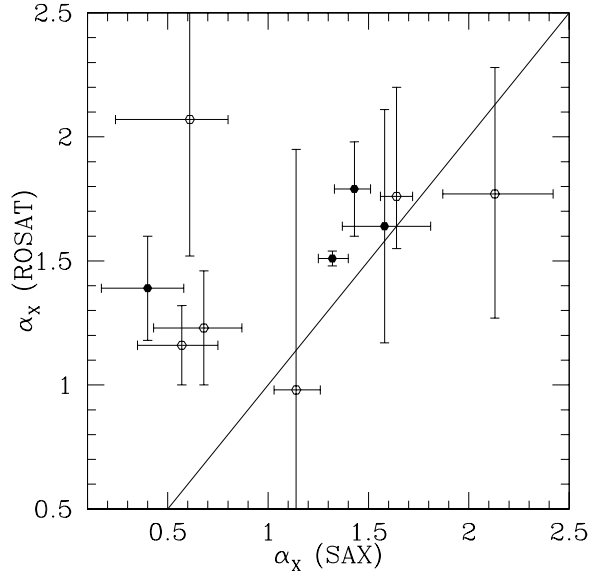


**Fig. 2.** X-ray spectral slopes derived from *BeppoSAX* in comparison to those from *ROSAT* PSPC data. The dashed line represents the  $\alpha_{BeppoSAX} = \alpha_{ROSAT}$  relation. Open symbols refer to the RASS-BSC data, while the others to *ROSAT* PSPC pointed observations. For objects where the broken-power law fit to the *BeppoSAX* spectra gave a better statistical result, the lower energy slope  $\alpha_1$  is reported.

by factors in the range  $F_{BeppoSAX} / F_{ROSAT} = 0.3 \dots 2.4$  with a mean ratio  $F_{BeppoSAX} / F_{ROSAT} = 1.1 \pm 0.7$ . Actually, high variability is expected in the X-ray flux of X-ray selected BL Lac objects (e.g. Mujica et al. 1999). It is interesting that for more radio powerful objects, like those belonging to the 1Jy sample, this ratio is inverted, with a measured mean ratio  $F_{BeppoSAX} / F_{ROSAT} = 0.6$  (Padovani et al. 2001). Radio selected BL Lac objects have flat inverse Compton spectra extending toward high energies (beyond  $\sim 1$  keV), but synchrotron emission, with a steep spectrum, may often dominate at soft energies. Therefore, the fit of their *BeppoSAX* LECS/MECS spectra, which sample a much wider energy range toward the high energies than the ROSAT PSPC spectra do, may be dominated by the flat inverse Compton component. Thus the fitted flux at 1 keV is lower than that determined with fits to ROSAT spectra. This might cause the low  $F_{BeppoSAX} / F_{ROSAT}$  ratio computed by Padovani et al. This problem does not affect the hard and flat soft X-ray spectra of our targets, so that our computed  $F_{BeppoSAX} / F_{ROSAT}$  ratio is consistent with unity.

The comparison between the ROSAT and *BeppoSAX* spectral slopes is shown in Figure 2. Again we used the spectral indices derived from the pointed PSPC observations if available and the RASS-BSC spectral slopes otherwise. In fact the best way would have been to fit the spectra in the same energy ranges for both instruments, as we did for the flux values. But we were prevented from doing so by the low statistics we would have had. The spectral slope

**Table 5.** ROSAT PSPC: Results for the pointed observations for two models: a single-power law with free fitted and with galactic absorption

Name	$F_X^a$	$N_{H,Fit}$	$F_{1keV}[\mu Jy]$	$\alpha_{ROSAT}^b$	$\chi_\nu^2(\text{d.o.f.})$	$N_{H,Gal}$	$\alpha_{ROSAT}^c$	$\chi_\nu^2(\text{d.o.f.})$	exp.time [sec]
1ES 0323+022	4.97	$9.7 \pm 0.3$	1.57	$1.64 \pm 0.47$	2.83 (17)	7.27	$1.39 \pm 0.25$	7.31 (18)	25304
1ES 0927+500	2.43	$2.6 \pm 0.4$	0.80	$1.39 \pm 0.13$	0.90 (17)	1.31	$0.92 \pm 0.06$	1.76 (18)	3831
1ES 1028+511	7.78	$1.4 \pm 0.7$	2.66	$1.51 \pm 0.03$	3.46 (17)	1.27	$1.43 \pm 0.01$	3.65 (18)	10777
1ES 1118+424	1.54	$2.6 \pm 0.3$	0.48	$1.79 \pm 0.12$	1.16 (17)	2.59	$1.79 \pm 0.03$	1.09 (18)	6416

<sup>a</sup> un-absorbed flux in the “hard” PSPC band (0.5–2.0 keV) in  $10^{-12}$  erg  $\text{cm}^{-2}\text{sec}^{-1}$

<sup>b</sup> spectral index for free fitted  $N_H$

<sup>c</sup> spectral index for  $N_H$  fixed to the Galactic value

**Table 6.** ROSAT PSPC: Results for the RASS data for two models: a single-power law with free fitted and with galactic absorption

Name	$F_X^a$	$N_{H,Fit}$	$F_{1keV}[\mu Jy]$	$\alpha_{ROSAT}^b$	$N_{H,Gal}$	$\alpha_{ROSAT}^c$	net counts <sup>d</sup>
1ES0323+022	12.3	18.9	1.49	$2.58^{+1.67}_{-1.03}$	7.27	$0.94^{+0.17}_{-0.21}$	$301.9 \pm 24.2$
1ES0507–040	9.3	8.8	2.54	$0.98^{+0.97}_{-0.82}$	7.84	$0.82^{+0.23}_{-0.27}$	$274.0 \pm 23.5$
1ES0927+500	18.1	2.2	2.57	$1.20^{+0.32}_{-0.31}$	1.31	$0.85^{+0.04}_{-0.04}$	$525.5 \pm 17.0$
1ES1028+511	18.0	1.5	4.52	$1.39^{+0.23}_{-0.22}$	1.27	$1.29^{+0.03}_{-0.03}$	$853.9 \pm 17.7$
1ES1118+424	4.7	3.3	0.80	$1.91^{+0.65}_{-0.62}$	2.59	$1.64^{+0.08}_{-0.08}$	$139.0 \pm 8.2$
1ES1255+244	4.8	3.8	0.34	$2.07^{+0.58}_{-0.55}$	1.21	$1.07^{+0.07}_{-0.07}$	$187.2 \pm 9.5$
1ES1533+535	8.0	2.0	1.82	$1.23^{+0.23}_{-0.23}$	1.28	$0.92^{+0.03}_{-0.03}$	$781.1 \pm 20.2$
1ES1544+820	4.0	5.3	1.26	$1.77^{+0.51}_{-0.50}$	3.70	$1.29^{+0.09}_{-0.09}$	$252.4 \pm 13.1$
1ES1553+113	12.0	0.7	3.64	$0.16^{+0.82}_{-0.40}$	3.53	$1.16^{+0.16}_{-0.16}$	$510.5 \pm 46.0$
1ES1959+650	27.9	15.8	1.23	$1.76^{+0.44}_{-0.21}$	0.99	$-0.60^{+0.03}_{-0.01}$	$3990.2 \pm 61.1$

<sup>a</sup> un-absorbed flux in the “hard” PSPC band (0.5–2.0 keV) in  $10^{-12}$  erg  $\text{cm}^{-2}\text{sec}^{-1}$

<sup>b</sup> spectral index for free fitted  $N_H$

<sup>c</sup> spectral index for  $N_H$  fixed to the Galactic value

<sup>d</sup> PSPC 0.5–2.0 keV band

values vary between the different observations, but the average difference is  $\alpha_{ROSAT} - \alpha_{BeppoSAX} = 0.0 \pm 0.4$  (if we consider only the objects with PSPC pointed observations we get  $\alpha_{ROSAT} - \alpha_{BeppoSAX} = 0.17 \pm 0.07$ , while for the RASS-BSC data  $\alpha_{ROSAT} - \alpha_{BeppoSAX} = -0.1 \pm 0.5$ ). While these spectral indices are consistent with each other it is remarkable that the broken-power law model applied to the *BeppoSAX* data shows in the low energy band ( $E < 1.5$  keV) a slope flatter than that of the *ROSAT PSPC* (0.1 – 2.4 keV). The difference might be a hint of more complex X-ray spectra or could result from the *ROSAT PSPC* calibration problems discussed by Iwasawa et al. (1999) and Barcons et al. (2000), who showed the X-ray spectral slopes measured by the *ROSAT PSPC* to be significantly steeper than those from other X-ray missions by  $\Delta\alpha_X \sim 0.4$ . PSPC spectra steeper than the *BeppoSAX* ones have also been found for the 1Jy sample (Padovani et al. 2001).

## 5. Spectral Energy Distribution

To determine the broadband SED of the 11 objects we used radio data at 1.4 GHz from the VLA surveys NVSS (Condon et al. 1998) or FIRST (White et al. 1997). Optical data were taken from the literature and for some

objects determined using the Calar Alto 1.23m telescope (Beckmann 2000a). A campaign for simultaneous optical data has also been performed for a few objects (Villata et al. 2000). Variability in the optical band is not expected to be large: all objects presented here are X-ray dominated objects (i.e.  $\alpha_{OX} < 1.2$ , see Table 7) which show only small optical variability (e.g. Villata et al. 2000, Mujica et al. 1999, Januzzi et al. 1994). With these data available we also computed the broad band spectral indices (between 1.4GHz, 4400 Å and 1 keV), which are reported in Table 7.

The following step consisted in parameterizing the derived SED.

Several authors pointed out that the synchrotron branch of the BL Lac SED can be well approximated by a parabolic spectral shape (cf. Landau et al. 1986, Comastri et al. 1995, Sambruna et al. 1996, Fossati et al. 1998, W98). We thus applied a parabolic fit to the SED in the  $\log \nu - \log \nu f_\nu$  plane – parameterized as  $\log \nu f_\nu = a \cdot (\log \nu)^2 + b \cdot \log \nu + c$  – and determined the peak position ( $\nu_{peak}$ ) and the total flux/luminosity of the synchrotron component. The resulting  $\nu_{peak}$  and two-point indexes are listed in Table 7. We also computed these quantities for

the objects reported in W98<sup>2</sup>. In the following discussion the whole sample of 21 BL Lac objects will be considered.

While the parabolic fits just described give a useful general parameterization of the SED, we have also considered all the available data and reproduced the SED of all sources of our sample with model dependent representations.

### 5.1. The blazar spectral sequence

Fossati et al. (1998) proposed a simple phenomenological description of the average SED of blazars, based on their bolometric observed luminosity which is in turn assumed to be well traced by the radio one. The latter in fact was found to correlate (and thus define) both the peak frequency of the synchrotron spectrum and the relative importance of the inverse Compton vs synchrotron powers. More recently, Donato et al. (2001) have revisited the original parameterization by Fossati et al. (1998), but (only) for objects below a radio luminosity of  $10^{43}$  erg  $s^{-1}$ , assuming a slightly different relation between the radio power, the synchrotron peak frequency and the inverse Compton luminosity. Thus in the Donato et al. (2001) model low power sources are assumed to have comparable luminosities in the synchrotron and self-Compton spectral components. We have then applied this parameterization to the objects in our sample, and the resulting ‘fits’<sup>3</sup> are shown as dashed lines in Fig. 3.

### 5.2. Homogeneous Synchrotron Self-Compton models

Finally we have reproduced the energy distributions adopting a more ‘physical’ approach by using an homogeneous (one-zone) synchrotron self-Compton model (this is a “one-zone version” of the model described in detail in Spada et al. 2001): it assumes that the source is cylindrical, of size  $R$  and width  $\Delta R' = R/\Gamma$  (in the comoving frame, here  $\Gamma$  is the bulk Lorentz factor). The model is aimed at reproducing the spectrum originating in a limited part of the jet, the one thought to be responsible for most of the emission. This region is necessarily compact, since it must account for the fast variability shown by all blazars, especially at high frequencies. Therefore the radio emission from these compact sources is strongly self-absorbed, and the model cannot account for the observed radio flux.

Sources in our sample are all BL Lacs of relatively low power with no signs of strong broad emission lines

<sup>2</sup> They slightly differ from the values presented there due to the different reference energies: our  $\alpha_{oz}$ ,  $\alpha_{ro}$  and  $\alpha_{rx}$  are lower by  $\sim 0.17$ ,  $\sim 0.05$ , and  $\sim 0.09$  than those presented in W98. Furthermore after the publication of W98 two more redshifts for objects of the sample have been determined, 1ES 0502+675 ( $z = 0.314$ , Scarpa et al. 1999) and 1ES 1517+656 ( $z = 0.702$ , Beckmann et al. 1999). Thus we lack only redshift information for 1ES 1544+820, for which we assume  $z = 0.2$ .

<sup>3</sup> Here not intended in a statistical sense, but only as approximate representations of the SEDs

in their spectra. Consequently, we have neglected the role of external seed photons for the inverse Compton (IC) process.

Relativistic electrons between a minimum and a maximum energy are injected throughout the source for a limited amount of time  $t_{inj}$  (mimicking a flare), which we set equal to  $t_{inj} = \Delta R'/c$ . High energy electrons whose radiative loss timescales are shorter than  $t_{inj}$  reach a stationary distribution, while lower energy electrons retain the original spectrum. The electron energies for which the cooling timescale is equal to  $t_{inj}$  are denoted by  $\gamma_c$ . The particle distribution  $N(\gamma)$  is assumed to have the slope  $n$  [ $N(\gamma) \propto \gamma^{-n}$ ] above  $\gamma_c$ , while below this value there can be two cases. We in fact assume that the particle distribution derives from a continuous injection of particles between  $\gamma_{min}$  and  $\gamma_{max}$ , and the slope below  $\gamma_c$  depends on whether  $\gamma_c$  is greater or smaller than  $\gamma_{min}$ . If  $\gamma_c > \gamma_{min}$ , we have  $N(\gamma) \propto \gamma^{-n+1}$  between  $\gamma_{min}$  and  $\gamma_c$  and  $N(\gamma) \propto \gamma^{-1}$  below  $\gamma_{min}$ . Alternatively, if  $\gamma_c < \gamma_{min}$ , then  $N(\gamma) \propto \gamma^{-2}$  between  $\gamma_c$  and  $\gamma_{min}$ . We further assume that, below the minimum between  $\gamma_c$  and  $\gamma_{min}$ ,  $N(\gamma) \propto \gamma^{-1}$ . According to these assumptions, the random Lorentz factor  $\gamma_{peak}$  of the electrons emitting most of the radiation (i.e. emitting at the peaks of the SEDs) becomes equal to  $\gamma_c$  and is determined by the importance of radiative losses and can assume values within the range  $\gamma_{min}-\gamma_{max}$ . Its value is listed in the last column of Table 8. The source is assumed to emit an intrinsic luminosity  $L'$  and is assumed to be observed with the viewing angle  $\theta$ . All these input parameters are listed in Table 8.

As can be noted from it, the intrinsic luminosities, the source dimensions, the bulk Lorentz factors and viewing angles, and the magnetic field values are very similar for all sources, in agreement with the fact that all objects belong to the same “flavor” of blazars. The resulting fits are shown in Fig. 3 as solid lines.

Let us compare these representations of the SEDs and in particular the results of the parameterization according to the Fossati et al (1998)’s scenario with those inferred from the homogeneous SSC model. It turns out that the former tends to overestimate the Compton  $\gamma$ -ray emission (by construction its power is never less than the synchrotron one), but it agrees with the existing upper limits in the GeV and TeV bands in all cases but 1ES 1553+113 and 1ES 1959+650. We stress that both these parameterizations are not meant to describe accurately the SED of specific sources, but only the average SED of sources of equal total power. Keeping this in mind, we can consider the difference between the two theoretical spectra for each source as a measure of the uncertainty associated with the ‘theoretical’ description of the SED.

### 5.3. Derived parameters and correlations

We can now consider possible trends in the properties of the SED and examine their consistency with the pre-

**Table 8.** Input parameters of the homogeneous synchrotron self-Compton model

Name	$L'$ erg s $^{-1}$	$R$ cm	$B$ G	$\Gamma$	$\theta$	$n$	$\gamma_{min}$	$\gamma_{peak}$
0145+146	$6.0 \times 10^{40}$	$8.0 \times 10^{15}$	1.0	11	5.0	3.8	600	27000
0323+022	$1.0 \times 10^{41}$	$1.0 \times 10^{16}$	0.9	11	3.7	3.5	800	27000
0507-040	$2.5 \times 10^{41}$	$1.0 \times 10^{16}$	1.2	15	3.5	3.3	1200	20000
0927+500	$6.0 \times 10^{41}$	$1.5 \times 10^{16}$	0.7	14	4.8	3.4	400	30000
1028+511	$2.7 \times 10^{41}$	$1.0 \times 10^{16}$	1.0	14	3.0	3.2	800	26000
1118+424	$2.0 \times 10^{41}$	$1.0 \times 10^{16}$	1.5	15	5.0	3.3	300	13000
1255+244	$6.5 \times 10^{41}$	$1.0 \times 10^{16}$	1.0	12	5.0	3.3	500	18000
1533+534	$1.5 \times 10^{42}$	$2.0 \times 10^{16}$	1.0	15	2.6	3.2	200	12000
1553+113	$2.5 \times 10^{42}$	$3.0 \times 10^{16}$	0.7	15	2.5	3.55	300	13000
1959+650	$8.0 \times 10^{40}$	$1.0 \times 10^{16}$	1.2	13	4.0	3.6	500	19000

**Table 7.** Derived quantities: Two-point broad band spectral indices<sup>a</sup>, X-ray luminosities and peak frequencies (for the 11 objects from this paper and for the 10 BL Lacs from W98).

Name	$\alpha_{ox}$	$\alpha_{ro}$	$\alpha_{rx}$	$\log L_X^b$	$\log(\nu_{peak})$
1ES 0145+138	1.19	0.41	0.65	43.42	14.49
1ES 0323+022	1.07	0.34	0.57	44.38	14.89
1ES 0507-040	0.69	0.52	0.58	45.26	18.05
1ES 0927+500	0.81	0.36	0.50	44.89	16.34
1ES 1028+511	0.81	0.33	0.48	45.86	16.08
1ES 1118+424	0.91	0.32	0.51	44.30	15.49
1ES 1255+244	1.14	0.15	0.46	44.88	15.09
1ES 1533+535	0.77	0.37	0.51	46.05	15.77
1ES 1544+820 <sup>c</sup>	0.71	0.47	0.55	44.11	16.15
1ES 1553+113	0.81	0.43	0.56	45.89	15.58
1ES 1959+650	1.05	0.31	0.54	44.11	15.00
MS 0158.5+0019	0.72	0.39	0.50	45.12	16.95
MS 0317.0+1834	0.64	0.42	0.49	45.11	18.51
1ES 0347-121	0.67	0.34	0.44	45.05	16.97
1ES 0414+009	0.76	0.42	0.53	45.59	16.25
1ES 0502+675	0.59	0.34	0.42	46.00	18.10
MS 0737.9+7441	0.84	0.39	0.54	44.93	15.72
1ES 1101-232	0.72	0.39	0.49	45.83	17.37
1ES 1133+704	1.04	0.43	0.62	43.69	14.96
MS 1312.1-4221	1.04	0.25	0.50	44.85	15.15
1ES 1517+656	0.75	0.32	0.47	46.55	16.17

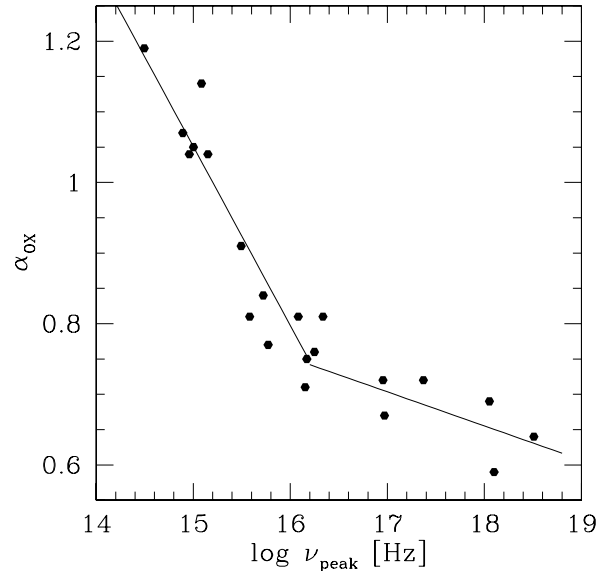
<sup>a</sup> derived from source fluxes at 1 keV, 4400 Å, and 1.4 GHz, resp.

<sup>b</sup> luminosity in the 2 – 10 keV band (MECS) in [erg/sec]

<sup>c</sup> assuming a redshift  $z = 0.2$

dictions of the blazar unifying scenario discussed above (Fossati et al 1998, Ghisellini et al 1998).

The first point we want to stress is that we find a strong correlation between  $\alpha_{ox}$  and the value of the peak frequency. The correlation is well represented by two linear regressions with a break around  $3 \times 10^{16}$  Hz as shown in Figure 4. (Note that small values of  $\alpha_{ox}$  refer to X-ray dominated objects while more optical dominated objects would have  $\alpha_{ox} > 1$ .) Indeed this result is similar to that

**Fig. 4.** X-ray dominance ( $\alpha_{ox}$ ) versus the peak frequency of the synchrotron branch. The more X-ray dominated objects have a higher peak frequency. The lines show two linear regression fits with a break at  $\log \nu_{peak} = 16.5$ .

found by Fossati et al. (1998) when studying the dependence of  $\alpha_{ro}$  and  $\alpha_{rx}$  on the peak frequency.

A second interesting trend appears to be present between the intrinsic absorption  $\Delta N_H \equiv N_{H,Fit} - N_{H,Gal}$  and the X-ray spectral slope  $\alpha_X$ . For all fits the value of the absorbing column was larger than the Galactic value. Even though error bars are large and part of the correlation might be spurious, there is indication of higher  $\Delta N_H$  for steeper X-ray spectra (Figure 5). If this trend were due to intrinsic absorption we should also find a correlation with the X-ray luminosity, which instead is not observed. Alternatively, in a single power law model the absorption can mimic an intrinsic curvature. Indeed a curvature of the X-ray spectra can easily account for the  $\Delta N_H$  vs  $\alpha_X$  behavior: near the synchrotron peak the spectra are harder and straighter than in the steep decay at frequencies higher than the peak. And in fact, the broken-power law model shows  $N_H$  values in agreement

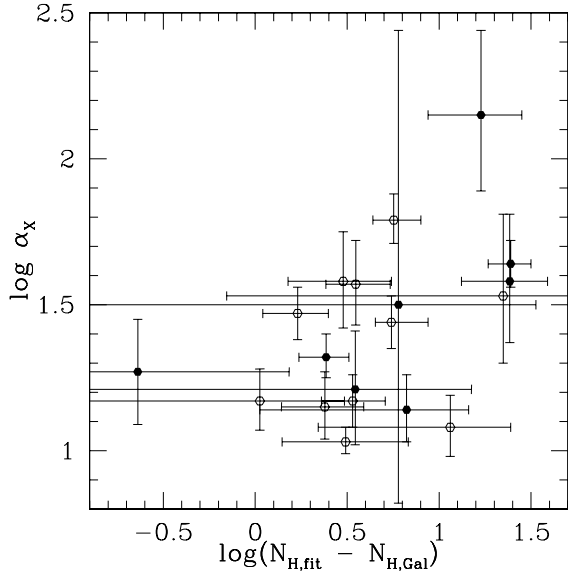


**Fig. 5.** Logarithmic “intrinsic” absorption ( $N_{H,Fit} - N_{H,Gal}$  in  $10^{20} \text{cm}^{-2}$ ) versus X-ray spectral slope. There is a trend for steeper spectra to correspond to higher “intrinsic” absorption. Filled symbols represent the cases where the single-power law fit was a better approximation to the *BeppoSAX* spectra than the broken-power law.

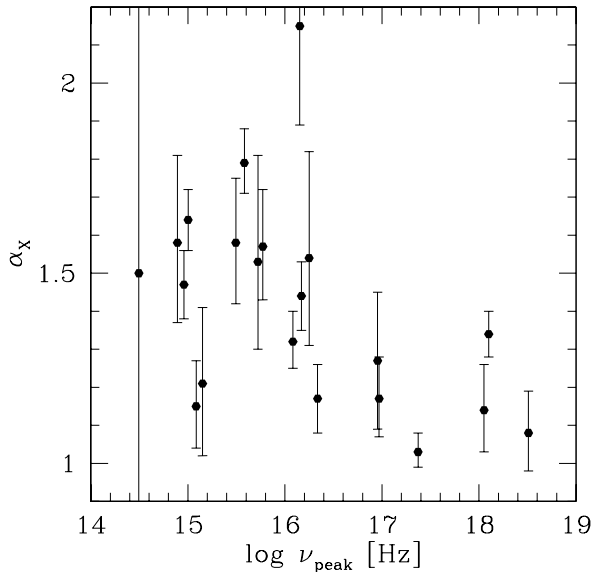


**Fig. 6.** X-ray spectral slope versus peak frequency.

with the Galactic hydrogen column density (when the *BeppoSAX* spectrum has enough counts to give a good statistics for this fit), and in all cases the value for a free fitted  $N_H$  for the pointed observations is in between the Galactic and the free fitted value from the single-power law. Furthermore we also find that a higher peak frequency is associated with a flatter spectral slope (Fig. 6), a trend that again can be accounted for by the above behavior: when the peak frequency is rising the X-ray band is located near the maximum of the synchrotron branch and this gives rise to flatter spectra.

A further correlation appears to be present between the X-ray dominance and the X-ray luminosity (Figure 7). Using a linear regression we find that it can be described as  $\log L_X = 47.7 - 3.2\alpha_{OX}$  with a correlation coefficient of 0.7. This cannot be due to selection effects (e.g. missing optical faint counterparts of the weaker X-ray sources). In this case there should be also a correlation between the X-ray *fluxes* and the X-ray dominance, but this is not detectable. This trend was already reported by Beckmann (1999, 2000) using a complete sample of BL Lac objects based on the RASS-BSC.

The same effect of X-ray dominated objects appearing to have X-ray luminosities higher than the intermediate BL Lacs should also be seen by comparing the peak frequency of the synchrotron branch with the X-ray luminosity. Within the scenario for the spectral properties of blazars discussed so far it should also be expected that as the objects considered here have similar radio power (i.e. total luminosity), their X-ray luminosity is bound to be mostly affected by the location of the synchrotron peak, higher energies corresponding to higher luminosities. However, contrary to these predictions, there does not seem to be a correlation between the peak frequency and the total luminosity of the synchrotron branch (as determined through the parabolic fit to the radio, optical and up to the X-ray data as described above). This might indicate that when objects of the same class are considered the range in total power is too small to show such a trend. The range of luminosities which is covered by the sample presented here is indeed small: the radio luminosity ranges from  $L_R = 1.2 \times 10^{24} \text{W/Hz}$  to  $L_R = 1.6 \times 10^{26} \text{W/Hz}$ , while the spread in the X-ray luminosity is one decade larger ( $1.4 \times 10^{19} \text{W/Hz} < L_X < 1.7 \times 10^{22} \text{W/Hz}$ ). For the radio, optical, and X-ray energy band studied here, we find an average of  $\log \nu L_R = 41.1 \pm 0.6$ ,  $\log \nu L_{Opt} = 44.7 \pm 0.6$ , and  $\log \nu L_X = 45.0 \pm 0.8$ , which are consistent with the average SEDs of HBL as shown by Fossati et al. (1998).

## 6. Discussion and Conclusions

The (physical) parameters of the objects studied here seem to partly correlate with the value of the peak frequency of the synchrotron branch of the SED. The X-ray selected sample considered in this work comprises objects whose synchrotron peaks are located near/in the X-ray band (high frequency peaked BL Lac, HBL; Padovani & Giommi 1996). Those of radio selected BL Lac objects tend instead to be located in the optical or infrared bands (low frequency peaked BL Lac, LBL), as is the case of sources belonging to the 1-Jy BL Lac sample (Stickel et al. 1991) whose peak frequencies can be as low as  $\sim 10^{13} \text{Hz}$  (Padovani et al. 2001).

We find a correlation between the peak frequency and the spectral slope as well as between the spectral slope and the flattening of the soft X-ray spectrum (parameterized as “intrinsic” absorption). These trends are consistent with the properties of the SED of HBLs: when the peak of the SED moves into the X-ray region the X-ray spectra



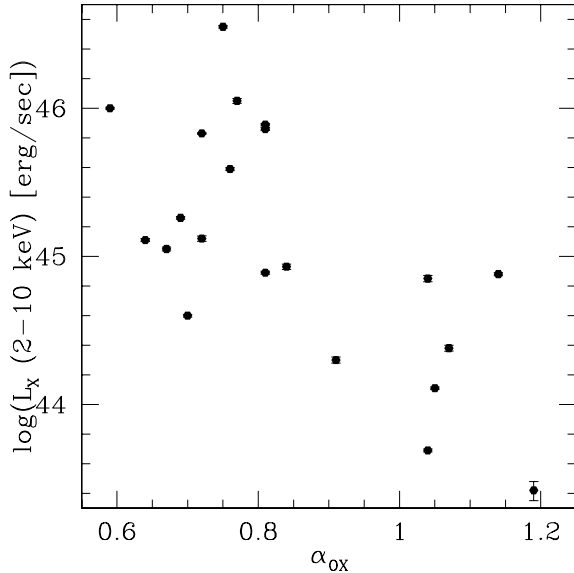


**Fig. 7.** X-ray luminosity for the *BeppoSAX* MECS band (2–10 keV) versus X-ray dominance ( $\alpha_{OX}$ ). Only for 1ES 0145+138 (bottom right) the error on the luminosity based on the count rate statistics is larger than the plotted symbol.

are expected to become harder and straighter as the peak frequency rises.

This behavior also accounts for the relative high X-ray luminosities observed in X-ray dominated BL Lacs (although LBL have higher total bolometric luminosities than HBL their X-ray emission corresponds to the energy band between the synchrotron and IC components, e.g. Fossati et al. 1998). Although within our sample it has not been possible to determine that HBL have lower bolometric luminosity (as a large fraction of the bolometric luminosity is expected to be emitted in the IC branch, which extends to energies outside the frequency range we covered), we can assume - as already mentioned - that the radio luminosity is a good tracer of the bolometric one (Fossati et al. 1998, Ghisellini 1999). The lack of a visible trend between such luminosities and the peak frequencies has then to be ascribed to the small luminosity range spanned by the HBL sample in comparison with the intrinsic dispersion of the peak-luminosity relation (as expected e.g. for a distribution of the observing viewing angle which tends to produce an opposite peak-luminosity trend).

If we consider this, the absence of correlation between the total luminosity in the synchrotron branch and the peak frequency will then result in higher bolometric luminosities for the LBL in comparison to the HBL. This is consistent with the fact that LBL show strong IC components compared to the synchrotron branch, while HBL emit similar luminosities in the IC and the synchrotron branch.

As the sample discussed here only includes HBL objects, we would expect the X-rays to be dominated by the higher energy part of the synchrotron and/or the lower

energy part of the IC component (Padovani et al. 2001, W98). Interestingly, no flattening associated with the latter component is observed up to several tens of keV (as the PDS data show that the X-ray power-law can be extended up to  $\sim 100$ keV), implying that the IC seems to start emerging at frequencies  $\nu > 10^{19}$ Hz. This is fully consistent with the assumed SED for HBL as inferred from the sequence scenario (Fossati et al. (1998).

In summary the *BeppoSAX* spectral survey shows that the X-ray properties of X-ray selected BL Lac objects are in good global agreement with the unified model for blazar, which ascribes the differences among blazars mostly to the location of the peak frequencies of the synchrotron and inverse Compton spectral components (e.g. Padovani & Giommi 1996, Ghisellini et al. 1998).

Even though the correlation of peak frequency with total luminosity as described by Fossati et al. (1998) cannot be found in this sample, we find that the spectral properties are fully consistent with objects having a spread in the position of the peak of the synchrotron branch around the X-ray band. The sample as a whole represents only a part of the blazar population. Comparing the luminosities in the different energy bands studied here, the objects match the average SEDs of HBL as shown by Fossati et al. (1998).

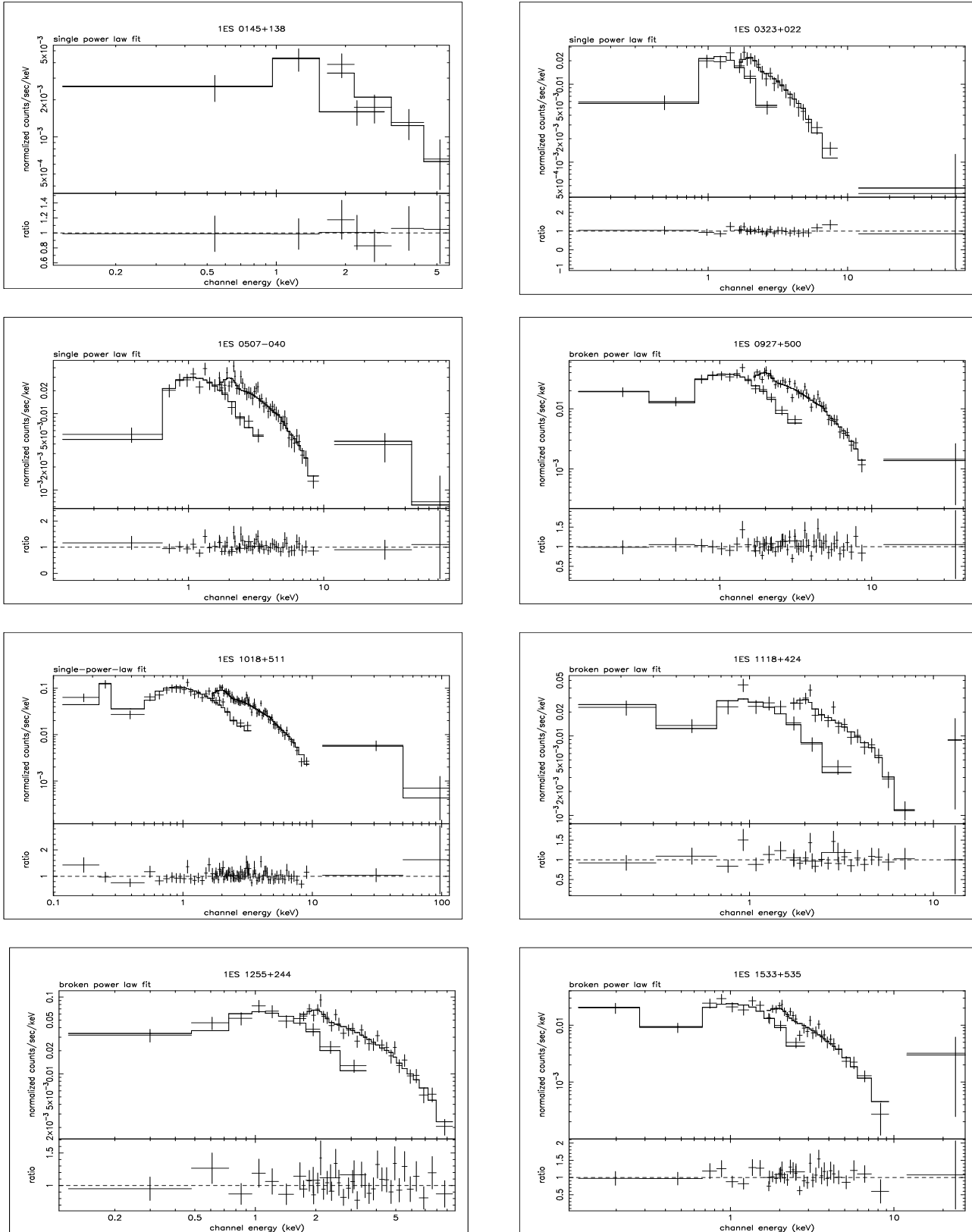
The energy coverage provided by *BeppoSAX* toward the high energies did not allow us to directly examine the link between the position of the peaks and the bolometric emitted power, as postulated by such model. Such study will be however possible with observations with sensitive instruments and good spectroscopy resolution above  $\sim 300$  keV as provided by e.g. the INTEGRAL mission, which will cover the energy range of the spectral change from the synchrotron to the IC dominated emission and possibly of the peak of the IC component.

*Acknowledgements.* We thank the referee Elena Pian for constructive comments, which helped to improve the manuscript. This research has made use of the NASA/IPAC Extragalactic Database (NED) which is operated by the Jet Propulsion Laboratory, California Institute of Technology under contract with the National Aeronautics and Space Administration. We thank Team Members of the *BeppoSAX* Science Operation Centre and Science Data Centre. The *BeppoSAX* program is supported by the Italian Space Agency ASI. VB thanks the *Osservatorio Astronomico di Brera* for the hospitality. This work has received partial financial support from the Deutsche Akademische Austauschdienst (DAAD), the Gruppo Nazionale di Astronomia of the CNR, and the Italian MURST.

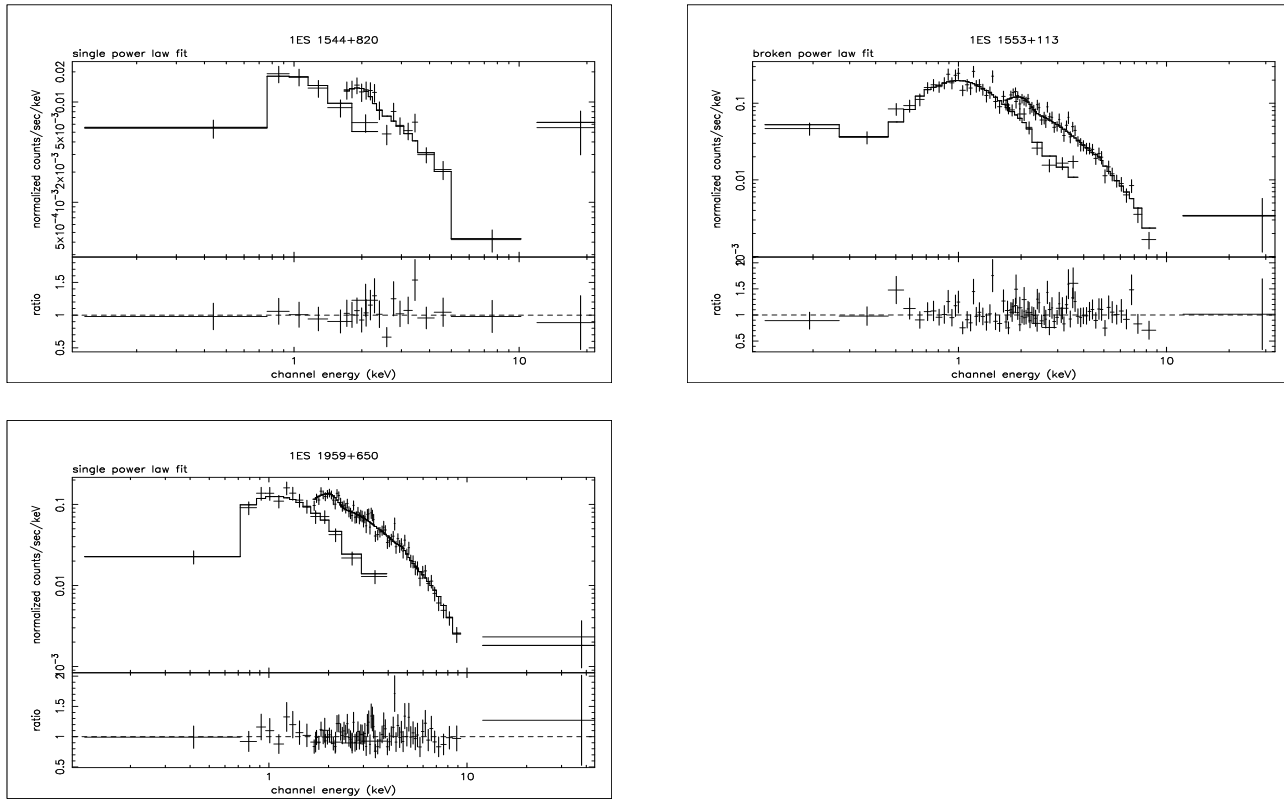
## References

- Bade N., Beckmann V., Douglas N. G., et al., 1998, *A&A* 334, 459
- Barcons X., Mateos S., Ceballos M. T., 2000, *MNRAS* 316, L13
- Beckmann V., 1999, in: *PASPC Vol. 159*, eds. L. O. Takalo, A. Silanpää
- Beckmann V., Bade N., Wucknitz O., 1999, *A&A* 352, 395

- Beckmann V., 2000, PhD thesis, Hamburg University, <http://www.sub.uni-hamburg.de/disse/330/vbdiss.html>
- Beckmann V., 2000a, BLAZAR Data 2, 3, <http://bldata.pg.infn.it/bldata.html>
- Boella G., Butler R. C., Perola G.C., et al., 1997, A&AS 122, 299
- Boella G., Chiappetti L., Conti G., et al., 1997b, A&AS 122, 327
- Brinkmann W., 1991, In: Physics of Active Galactic Nuclei, Proceedings of the International Conference, Heidelberg, 3.-7.June 1991, Eds. Duschl, W. J., Wagner, S.J.
- Butler C., Scarsi L., 1990, SPIE 1344, 46
- Comastri A., Molendi S., and Ghisellini G., 1995, MNRAS 277, 297
- Condon J. J., Cotton W. D. Greisen E. W., et al. 1998, AJ 115, 1693
- Donato D., Ghisellini G., Tagliaferri G., Fossati G., 2001, A&A 375, 739
- Fossati G., Maraschi L., Celotti A., et al., 1998, MNRAS 299, 433
- Ghisellini G., Celotti A., Fossati G., et al., 1998, MNRAS 301, 451
- Ghisellini G., 1999, in PASPC Vol. 159, eds. L. O. Takalo, A. Silanpää, p. 311
- Gioia I. M., Maccacaro T., Schild R. E., et al., 1990, ApJS 72, 567
- Hartmann D., Burton W.B., 1997, "Atlas of Neutral Galactic Hydrogen", Cambridge University Press, Cambridge, New York
- Iwasawa K., Fabian A. C., Nandra K., 1999, MNRAS 307, 611
- Januzzi, B. T., Smith, P. S., Elstan, R., 1994, ApJ 428, 130
- Kühr H., Schmidt G. D., 1990, AJ 99, 1
- Landau R., Golisch B., Jones T. J., et al., 1986, ApJ 308, 78
- Morrison R., Mc Cammon D., 1983, ApJ 270, 119
- Mujica R., Appenzeller F.-J., Krautter I., et al., 1999, in: PASPC Vol. 159, eds. L. O. Takalo, A. Silanpää
- Orr A., Parmar A. N., Yaqoob T., Guainazzi M., 1998, in: Proceedings of the Active X-ray Sky symposium, October 21-24, 1997, Rome, eds. Scarsi et al.
- Padovani P., Costamante L., Giommi P., et al., 2001, MNRAS 328, 931
- Padovani P., Giommi P., 1996, MNRAS 279, 526
- Parmar A.N., Martin D.D.E., Bavdaz M., et al., 1997, A&AS 122, 309
- Perlman E. S., Stocke J. T., Schachter J. F., et al., 1996, ApJS 104, 251
- Sambruna R. M., Maraschi L., Urry C. M., 1996, ApJ 463, 444
- Scarpa R., Urry C. M., Falomo R., et al., 1999, ApJ 521, 134
- Scarpa R., Urry C. M., Falomo R., et al., 2000, ApJ 532, 74
- Schartel N., Walter R., Fink H. H., Trümper J., 1996, A&A 307,33
- Spada M., Ghisellini G., Lazzati D., Celotti A., 2001, MNRAS 325, 1559
- Stickel M., Padovani P., Urry C. M., et al., 1991, ApJ 374, 431
- Stocke J. T., Morris S. L., Gioia I. M., et al., 1991, ApJS 76, 813
- Villata M., Raiteri C. M., Popescu M. D., et al., 2000, A&AS 144, 481
- Voges W., 1992, in: Proceedings on European International Space Year Meeting ESA ISY-3, 9
- Voges W., Aschenbach B., Boller Th., et al., 1999, A&A 349, 389
- Wagner S. J., Witzel A., 1995, ARA&A 33, 163
- White R. L., Becker R. H., Helfand D. J., Gregg M. D., 1997, ApJ 475, 479
- Wolter A., Comastri A., Ghisellini G., et al., 1998, A&A 335, 899 (W98)



**Fig. 1.** Fits to the *BeppoSAX* spectra. In the five cases where it gives a better spectral fit the result of the broken-power law fit is shown.

**Fig. 1.** (continued)

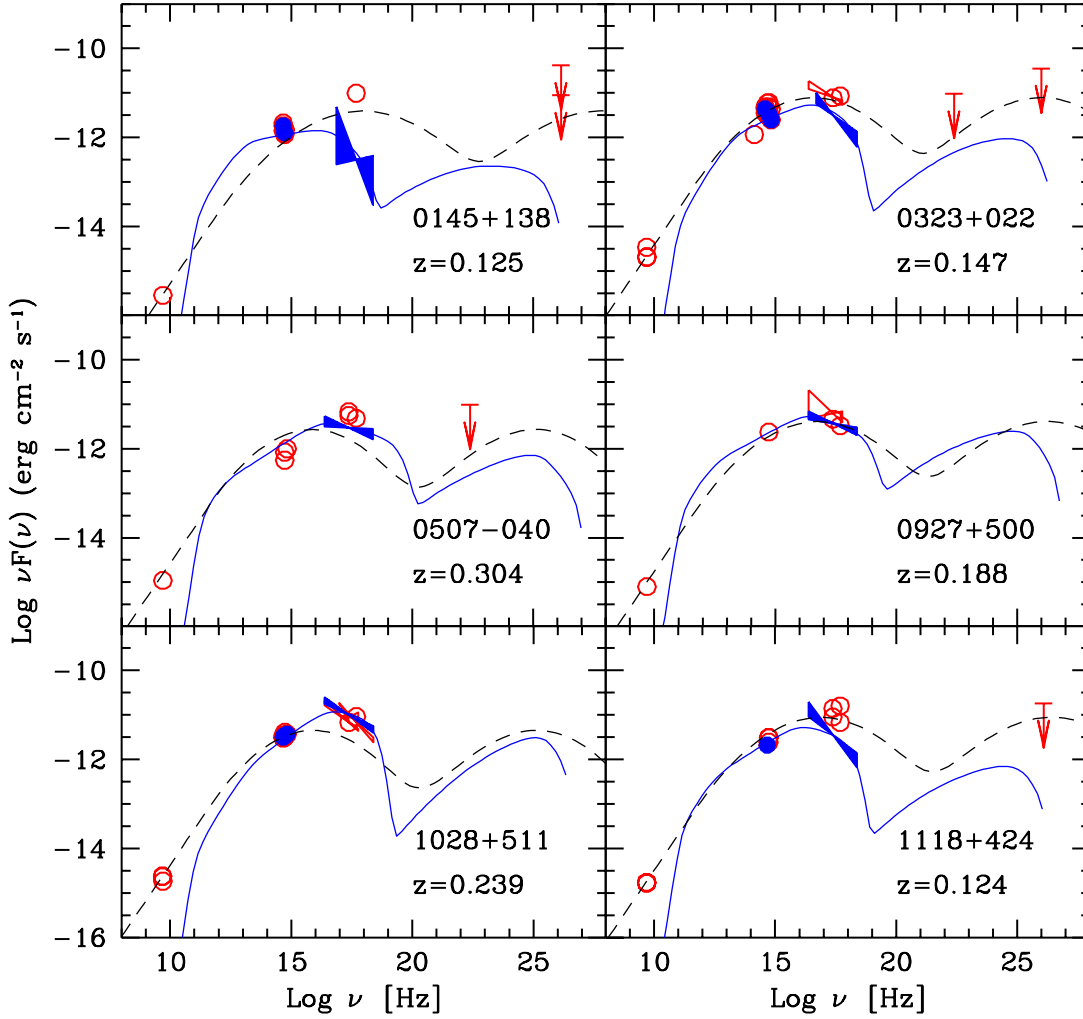


**Fig. 3.** Spectral energy distribution of our sources. The solid lines correspond to the one-zone homogeneous synchrotron and inverse Compton model calculated as explained in the text, with the parameters listed in Table 8. The dashed lines represent instead the spectrum predicted by the phenomenological SED description by Fossati et al. (1998) (with the changes proposed by Donato et al. 2001). The *BeppoSAX* data and simultaneous optical data of our observing campaigns are indicated by the filled bow-ties and symbols.

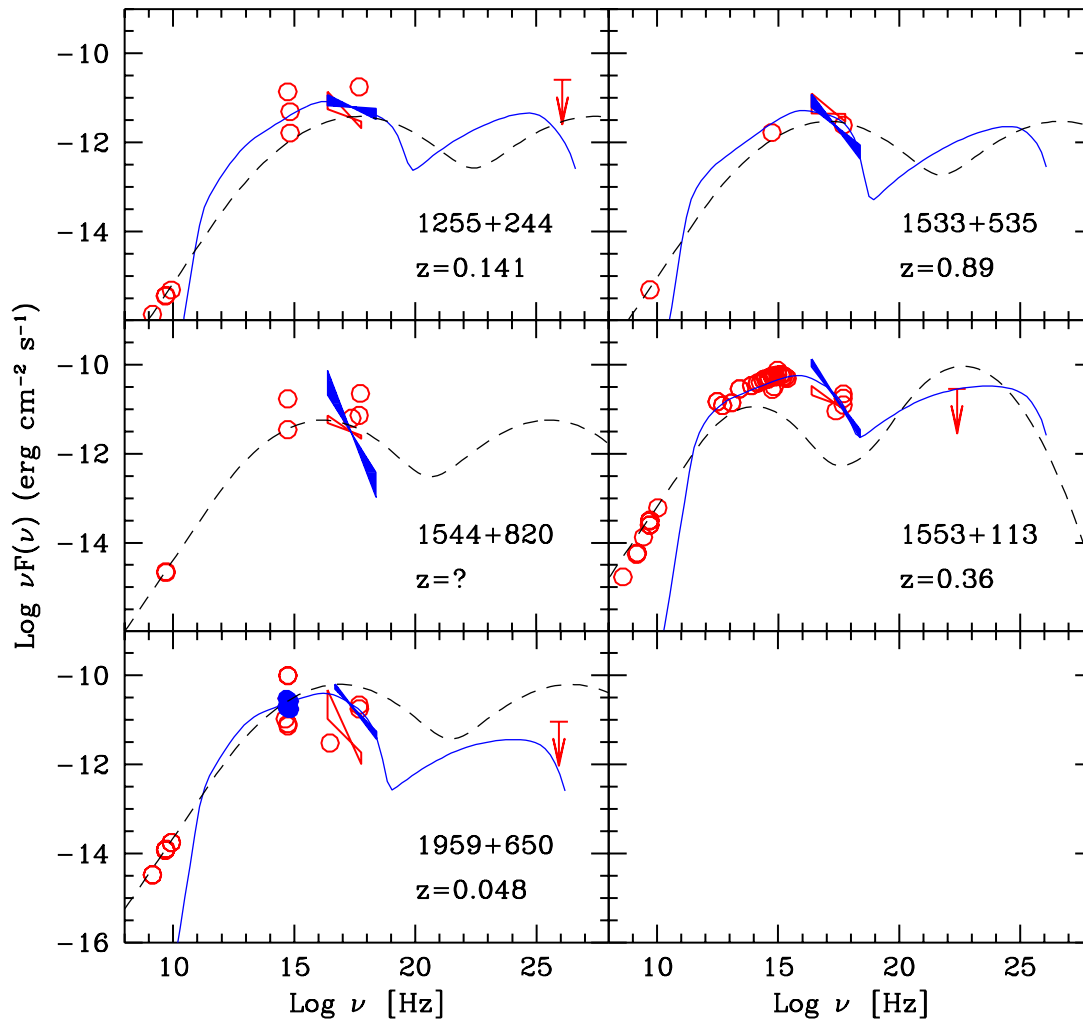


Fig. 3. (continued)